Global Energy Interconnection 9 (2026) 108–118

KeAi
CHINESE ROOTS
GLOBAL IMPACT

Global Energy Interconnection
Development and Cooperation Organization

Global Energy Interconnection

Contents lists available at ScienceDirect
journal homepage: www.elsevier.com/locate/gloei

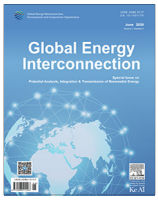

An evaluation method for the aggregate adjustable capability of photovoltaic-storage-charging stations considering local security constraints

Chao Li [a], Jiawei He [b,*], Tingzhe Pan [c], Zijie Meng [a], Xinlei Cai [a], Xin Jin [c], Zechun Hu [b]

[a] *Power Dispatching Control Center of Guangdong Power Grid Co. Ltd, Guangzhou 510600, China*
[b] *Department of Electrical Engineering, Tsinghua University, Beijing 100084, China*
[c] *CSG Electric Power Research Institute, Guangzhou 510663, China*

Received 14 September 2025; revised 31 October 2025; accepted 11 November 2025

Abstract

As renewable energy penetration continues to rise, enhancing power system flexibility has become a critical requirement. Photovoltaic–storage–charging stations (PSCSs) are key components for enhancing local regulation capability and promoting renewable integration. However, evaluating the adjustable capability of such hybrid stations while considering security constraints remains a major challenge. This paper first analyzes the adjustable capabilities of all the resources within such a station based on the power-energy boundary (PEB) model. Then, an optimal formulation is proposed to obtain the adjusted parameters of the aggregate feasible region (AFR) model, which embeds low-dimensional linear models within high-dimensional linear models to improve the accuracy. To solve this formulation, it is transformed using duality theory and an alternating optimization algorithm is designed to obtain the solution. Finally, a multi-station adjustable capability aggregation method considering security constraints is introduced. Simulation results verify that the proposed method effectively reduces infeasible regions and improves smoothness of aggregated boundaries, providing an accurate and practical tool for flexibility evaluation in PSCSs and offering guidance for aggregators and system planners.

Keywords: Photovoltaic; Energy storage; Electric vehicle charging station; Flexibility aggregation

0 Introduction

With the rapid development of renewable energy in China, the share of renewable energy in the power system continues to grow, which imposes higher demands on the system's flexibility. A photovoltaic–storage–charging station (PSCS) consists of three types of controllable resources: photovoltaics (PV), energy storage systems (ESS), and electric vehicle (EV) charging facilities. Through appropriate control strategies, such stations can improve the utilization of renewable energy, reduce operational costs and carbon emissions [1,2], and they can also participate in power system optimization to obtain additional economic benefits [3]. To fully leverage the potential of PSCSs, it is necessary for an aggregator or a virtual power plant (VPP) operator to establish an aggregation model to assess the total adjustable capability of these resources.

Currently, research on PSCSs mainly focuses on siting and sizing planning as well as operation and control strategies [4], whereas systematic evaluation methods for their

Peer review under the responsibility of Global Energy Interconnection Group Co. Ltd.
* Corresponding author.
E-mail addresses: lx_lichao47@163.com (C. Li), hejw24@mails.tsinghua.edu.cn (J. He), pantz@csg.cn (T. Pan), meteordk@163.com (Z. Meng), 517665114@qq.com (X. Cai), jinxin1@csg.cn (X. Jin), zechhu@tsinghua.edu.cn (Z. Hu).

https://doi.org/10.1016/j.gloei.2025.11.002

adjustable capability remain to be further developed. As one of the primary user-oriented flexible resources in such stations, EV charging facilities have already been widely studied in terms of controllability modeling and aggregation assessment. References [5,6] established time-sequential controllability models for parked EVs and EV battery swapping stations using clustering and recursive approaches, deriving the time-sequential controllable power boundaries of EV clusters. Reference [7] developed an EV aggregation model based on Monte Carlo simulation and Markov chains, considering user randomness and socio-economic diversity. Reference [8] proposed a time-varying storage model to describe the flexibility of large-scale EV charging facilities and applied it to forecasting and control problems. Reference [9] simplified the computation of EV cluster flexibility by applying affine transformations to the flexibility polytope of individual EVs and reformulated the maximum volume inner-approximation problem into a tractable linear problem.

Regarding the aggregation modeling of more general distributed flexible resources, from the perspective of whether geographic distribution and network constraints are considered, the published methods can be categorized into station-level aggregation and network-level aggregation. The purpose of station-level aggregation is typically to obtain the total adjustable capability of a single station. Main approaches include polytope-based methods, Monte Carlo simulations, and data-driven methods. Reference [10] employed homothetic polytopes, approximating feasible regions of individual resources through translation and scaling operations, thereby simplifying Minkowski sum calculations. Reference [11] proposed an exact algorithm for converting between the polytope form and the zonotope form of feasible regions, leveraging the computational advantages of zonotopes in Minkowski sums, while improving approximation accuracy through optimal generator selection. Reference [12] effectively solved the inner-approximation problem of feasible regions by vertex contraction, applying it to the security-constrained unit commitment problem to reduce the power system operating cost. Reference [13] argued that template geometry-based methods are unsuitable for industrial loads with integer variables, and therefore proposed a data-driven dimensionality reduction model trained on industrial load data, enhancing adaptability to integer variables.

For network-level aggregation, common approaches include random sampling, mathematical optimization, and polytope contraction methods. Reference [14] compared the feasible regions of distribution networks with network constraints obtained by random sampling and optimal power flow methods, showing that the former is more suitable for small-scale grids. Reference [15] proposed a robust capability curve model to describe the maximum active and reactive power outputs of VPP, estimating parameters using the convex hull of boundary points. Reference [16] developed a two-stage optimization model: in the first stage, constraints of distributed resources were aggregated to their connected nodes; in the second stage, an optimization model incorporating nodal constraints, branch capacities, and network constraints was formulated. Reference [17] employed adaptive robust optimization to obtain the active–reactive elliptical feasible region of VPP. Reference [18] established a stochastic flexibility evaluation model for VPP, which can be directly applied to unit commitment and economic dispatch problems.

In summary, the current evaluation methods of adjustable capability for PSCSs face issues such as computational complexity, inaccuracy of evaluation results, and the neglect of local constraints. In particular, most existing aggregation approaches only provide overly simplified approximations of the feasible region, which cannot accurately capture the actual decomposability of aggregated power. Moreover, few studies explicitly incorporate local transformer or substation capacity limits into the flexibility evaluation framework. To address these gaps, this paper develops an improved evaluation method that embeds low-dimensional boundaries into high-dimensional models to obtain tighter outer approximations. In addition, a two-stage aggregation framework is proposed to consider local security constraints, ensuring both accuracy and practical applicability in real-world operations.

The remainder of this paper is organized as follows. Section 1 introduces the modeling framework for the adjustable capability of a single PSCS based on power–energy boundaries. Section 2 establishes the improved aggregate feasible region (AFR) model and develops the alternating optimization algorithm for solving it. Section 3 extends the method to multi-station aggregation considering local security constraints. Section 4 provides case studies. Finally, Section 5 concludes the paper.

To improve readability, key terms and abbreviations used throughout the paper are summarized in Table 1.

1 Modeling of adjustable capability of a single PSCS based on power-energy boundaries

1.1 Modeling of individual resource adjustable capability

This section mainly discusses the modeling of adjustable capability for various resources within a PSCS. According to the power-energy boundary (PEB) models of distributed resources [19,20], the adjustable capability of a single resource can be represented by a four-tuple $(\overline{p}^{t}_{i,j}, \underline{p}^{t}_{i,j}, \overline{e}^{t}_{i,j}, \underline{e}^{t}_{i,j})$, which respectively denotes the upper and lower bounds of the power and cumulative consumed energy of the j-th resource in station i. Let the power of the j-th resource in station i at time t be $p^{t}_{i,j}$, then:

Table 1
Key terms and abbreviations.

Term	Explanation
Aggregate Feasible Region (AFR)	The feasible region of the aggregated power.
AFR-1′ / AFR-2	Two approximate models of the exact aggregate feasible region [21], both providing outer approximations, with AFR-2 being more accurate than AFR-1′.
Power–Energy Boundary (PEB)	A pair of upper and lower bounds describing the maximum and minimum achievable power and cumulative energy trajectories of an individual resource.
Guidance Power (p_*^t)	The target or reference power trajectory obtained from optimization, used to guide operational scheduling.

$$\underline{p}_{i,j}^{t} \le p_{i,j}^{t} \le \bar{p}_{i,j}^{t}, \forall t \in \{1,2,...,T_{\mathrm{d}}\} \tag{1}$$

$$\underline{e}_{i,j}^{t} \le \delta \sum_{\tau=1}^{t} p_{i,j}^{\tau} \le \bar{e}_{i,j}^{t}, \forall t \in \{1,2,...,T_{\mathrm{d}}\} \tag{2}$$

where T_{d} Td is the total number of time intervals in a day, and δ is the length of one interval. Next, the resources within a PSCS are modeled by converting their adjustable capabilities into the four-tuple form.

1.1.1 PV

The PV resource can be regarded as negative stochastic loads, where the power can be adjusted between 0 and the actual generated power. Therefore, the upper bound of power ($\bar{p}_{i,j}^{t}$) is 0, and the lower bound ($\underline{p}_{i,j}^{t}$) is the negative of its output curve. In this paper, a unified description is adopted using the four-tuple of power-energy boundaries, with cumulative energy upper and lower bounds calculated as follows:

$$\bar{e}_{i,j}^{t} = \delta \sum_{\tau=1}^{t} \bar{p}_{i,j}^{\tau} = 0, \forall t \in \{1,2,...,T_{\mathrm{d}}\} \tag{3}$$

$$\underline{e}_{i,j}^{t} = \delta \sum_{\tau=1}^{t} \underline{p}_{i,j}^{\tau}, \forall t \in \{1,2,...,T_{\mathrm{d}}\} \tag{4}$$

1.1.2 ESS

ESS is a time-coupled flexible resource. Assume the rated power be $P_{i,j}^{\mathrm{ES}}$, charging and discharging efficiencies be $\eta_{i,j}^{\mathrm{c}}$ and $\eta_{i,j}^{\mathrm{d}}$, energy capacity be $B_{i,j}^{\mathrm{ES}}$, and the initial state of charge (SoC) at the time of evaluation be $S_{\mathrm{OC},i,j}^{\mathrm{ES,a}}$, respectively. The maximum and minimum safe SoC, considering safety and lifetime factors, are $S_{\mathrm{OC},i,j}^{\mathrm{ES,max}}$ and $S_{\mathrm{OC},i,j}^{\mathrm{ES,min}}$, respectively. The power boundaries of ESS during the considered period are given as follows:

$$\bar{p}_{i,j}^{t} = P_{i,j}^{\mathrm{ES}}, \forall t \in \{1,2,...,T_{\mathrm{d}}\} \tag{5}$$

$$\underline{p}_{i,j}^{t} = -P_{i,j}^{\mathrm{ES}}, \forall t \in \{1,2,...,T_{\mathrm{d}}\} \tag{6}$$

The cumulative energy boundaries of ESS are illustrated in Fig. 1. The upper boundary represents the fastest charging trajectory: continuous charging from the initial period until the maximum safe energy is reached, followed by discharging at maximum power to ensure the end-period energy level matches that of the initial period. The lower boundary represents the fastest discharging trajectory: continuous discharging from the initial period until the minimum safe energy is reached, followed by charging at maximum power to maintain the end-period energy at the same level as the initial period. The maximum and minimum cumulative consumed energy are given by (7) and (8).

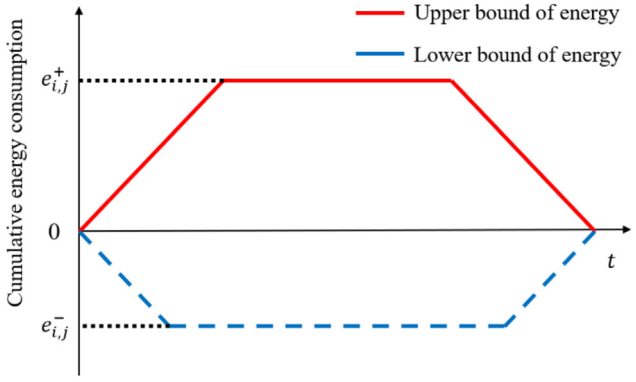

Fig. 1. Cumulative energy boundaries of ESS.

$$e_{i,j}^{+} = B_{i,j}^{\mathrm{ES}} \left(S_{\mathrm{OC},i,j}^{\mathrm{ES,max}} - S_{\mathrm{OC},i,j}^{\mathrm{ES,a}} \right) \tag{7}$$

$$e_{i,j}^{-} = B_{i,j}^{\mathrm{ES}} \left(S_{\mathrm{OC},i,j}^{\mathrm{ES,min}} - S_{\mathrm{OC},i,j}^{\mathrm{ES,a}} \right) \tag{8}$$

1.1.3 EV

An EVs is also a time-coupled flexible resource. Let its arrival time and SoC at the charging station be $t_{i,j}^{\mathrm{a}}$ and $S_{\mathrm{OC},i,j}^{\mathrm{EV,a}}$, the expected departure time and target SoC be $t_{i,j}^{\mathrm{d}}$ and $S_{\mathrm{OC},i,j}^{\mathrm{EV,d}}$, the rated charging power be $P_{i,j}^{\mathrm{EV}}$, and the battery capacity be $B_{i,j}^{\mathrm{EV}}$, respectively. The power boundaries restrict the maximum charging power during the adjustable period as follows:

$$\bar{p}_{i,j}^{t} = \begin{cases} P_{i,j}^{\mathrm{EV}}, t \in \left[t_{i,j}^{\mathrm{a}}, t_{i,j}^{\mathrm{d}} \right] \\ 0, t \notin \left[t_{i,j}^{\mathrm{a}}, t_{i,j}^{\mathrm{d}} \right] \end{cases} \tag{9}$$

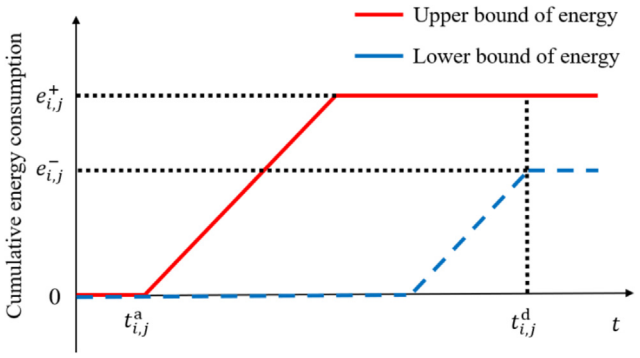

Fig. 2. Cumulative energy boundaries of EV.

$$\underline{p}^{t}_{i,j} = 0 \tag{10}$$

The cumulative energy boundaries are shown in Fig. 2. The upper boundary represents the fastest charging trajectory: continuous charging from the connection time until the maximum capacity is reached. The lower boundary represents the slowest charging trajectory: no charging immediately after connection, followed by charging starting at a certain time, so that the target SoC is reached exactly by the departure time. The energy consumed under these two trajectories is calculated by (11) and (12).

$$e^{+}_{i,j} = B^{\mathrm{EV}}_{i,j}\left(1 - S^{\mathrm{EV,a}}_{\mathrm{OC},i,j}\right) \tag{11}$$

$$e^{-}_{i,j} = B^{\mathrm{EV}}_{i,j}\left(S^{\mathrm{EV,d}}_{\mathrm{OC},i,j} - S^{\mathrm{EV,a}}_{\mathrm{OC},i,j}\right) \tag{12}$$

1.2 Adjustable capability model of a single PSCS

Let Φ^{sta}_{i} denote the set of resources connected to the i-th PSCS. By summing the four-tuple parameters of all resources at station i, the aggregated power and energy boundaries of station i can be obtained by (13)–(16), which corresponds to the AFR-1′ model in [21]. This model provides an outer approximation of the exact feasible region, with the advantages of simple computation. However, it may contain a certain proportion of infeasible points, which prevents the total power from being successfully allocated to individual resources, thereby limiting its practical applicability.

$$\bar{P}^{t}_{i} = \sum_{j\in\Phi^{\mathrm{sta}}_{i}} \bar{p}^{t}_{i,j} \tag{13}$$

$$\underline{P}^{t}_{i} = \sum_{j\in\Phi^{\mathrm{sta}}_{i}} \underline{p}^{t}_{i,j} \tag{14}$$

$$\bar{E}^{t}_{i} = \sum_{j\in\Phi^{\mathrm{sta}}_{i}} \bar{e}^{t}_{i,j} \tag{15}$$

$$\underline{E}^{t}_{i} = \sum_{j\in\Phi^{\mathrm{sta}}_{i}} \underline{e}^{t}_{i,j} \tag{16}$$

2 Improved model of adjustable capability for a single PSCS

2.1 Improved model based on set inclusion

To reduce the infeasible region of aggregated adjustable capability evaluation at a single station by AFR-1′ model, this paper adopts the more accurate AFR-2 model from [21] to improve the performance of the AFR-1′ model. The AFR-2 model is formulated as follows:

$$\begin{aligned}&\sum_{j\in\Phi^{\mathrm{sta}}_{i}} \max\left(\underline{e}^{t_1}_{i,j} - \bar{e}^{t_2}_{i,j}, \sum_{\tau=t_2+1}^{t_1} \underline{p}^{\tau}_{i,j}\delta\right) \le E^{t_1}_{i} - E^{t_2}_{i} \\ &\le \sum_{j\in\Phi^{\mathrm{sta}}_{i}} \min\left(\bar{e}^{t_1}_{i,j} - \underline{e}^{t_2}_{i,j}, \sum_{\tau=t_2+1}^{t_1} \bar{p}^{\tau}_{i,j}\delta\right), \\ &t_1 \in [1, T_{\mathrm{d}}], t_2 \in [0, t_1 - 1],\end{aligned} \tag{17}$$

where E^{t}_{i} is the cumulative consumed energy of station i at time period t, and the cumulative consumed energy at the initial moment (E^{0}_{i}) equals 0. It can be seen that this model restricts the difference of cumulative consumed energy between any two time intervals, but does not provide intuitive upper and lower boundaries of power and energy at each time. The number of constraints in the AFR-2 model (n_{c2}) is much larger than that in the AFR-1′ model ($n_{\mathrm{c1}'}$). For example, when$T_{\mathrm{d}} = 96$, n_{c2}=97*96 = 9312 and$n_{\mathrm{c1}'}$ = 96*4 = 384. Therefore, we take the AFR-1′ model as the optimization target, adjusting its parameters so that its corresponding boundaries is compressed into the feasible region of the AFR-2 model, thereby obtaining the improved boundary parameters.

First, both the AFR-2 model and the AFR-1′ model are rewritten into linear inequality systems with as the variable:

$$\mathrm{AFR}\text{ - }2 : \left\{\boldsymbol{E}_i \in \mathbb{R}^{T_{\mathrm{d}}+1} \middle| \mathbf{A}\boldsymbol{E}_i \le \boldsymbol{b}_i\right\} \tag{18}$$

$$\mathrm{AFR} - 1\prime : \left\{\boldsymbol{E}_i \in \mathbb{R}^{T_{\mathrm{d}}+1} \middle| \boldsymbol{C}\boldsymbol{E}_i \le \boldsymbol{d}_i\right\} \tag{19}$$

where matrix $\mathbf{A}$ and vector $\boldsymbol{b}_i$ are generated according to (17) by traversing t_1 and t_2, respectively. $\mathbf{A} \in \mathbb{R}^{T_{\mathrm{d}}(T_{\mathrm{d}}+1)\times(T_{\mathrm{d}}+1)}$, $\boldsymbol{b} \in \mathbb{R}^{T_{\mathrm{d}}(T_{\mathrm{d}}+1)}$. Matrix $\mathbf{C}$ is composed of the identity matrix $\mathbf{I}$ and the Jordan matrix $\mathbf{D}$, where the diagonal entries of $\mathbf{D}$ are 1, the sub-diagonal entries are –1, and all other elements are 0.

$$\mathbf{C} = \begin{bmatrix} \mathbf{I} \\ -\mathbf{I} \\ \mathbf{D} \\ -\mathbf{D} \end{bmatrix} \in \mathbb{R}^{4(T_{\mathrm{d}}+1)\times(T_{\mathrm{d}}+1)} \tag{20}$$

$$\mathbf{D} = \begin{bmatrix} 1 & 0 & 0 & 0 \\ -1 & 1 & 0 & 0 \\ \cdots & \ddots & \ddots & \cdots \\ 0 & 0 & -1 & 1 \end{bmatrix} \in \mathbb{R}^{(T_{\mathrm{d}}+1)\times(T_{\mathrm{d}}+1)} \tag{21}$$

In (19), vector $\boldsymbol{d}_i$ is the variable to be optimized. When matrix $\mathbf{C}$ takes the form of (20), the meaning of $\boldsymbol{d}_i$ is as follows:

$$\boldsymbol{d}_i = \begin{bmatrix} \bar{\boldsymbol{E}}_{i,\mathrm{opt}} \\ -\underline{\boldsymbol{E}}_{i,\mathrm{opt}} \\ \delta\bar{\boldsymbol{P}}_{i,\mathrm{opt}} \\ -\delta\underline{\boldsymbol{P}}_{i,\mathrm{opt}} \end{bmatrix} \in \mathbb{R}^{4(T_\mathrm{d}+1)} \tag{22}$$

where $\bar{\boldsymbol{E}}_{i,\mathrm{opt}}$ and $\underline{\boldsymbol{E}}_{i,\mathrm{opt}}$ represent the optimized upper and lower bounds of cumulative consumed energy, and $\bar{\boldsymbol{P}}_{i,\mathrm{opt}}$ and $\underline{\boldsymbol{P}}_{i,\mathrm{opt}}$ represent the optimized upper and lower bounds of power, respectively. The objective function of the optimization problem is defined as:

$$\min \sum_{t=1}^{T_\mathrm{d}} \left(L_1^t + \beta L_2^t\right) \tag{23}$$

$$\begin{aligned} L_1^t = &\left(\bar{E}_{i,\mathrm{opt}}^t - \bar{E}_i^t\right)^2 + \left(\underline{E}_{i,\mathrm{opt}}^t - \underline{E}_i^t\right)^2 \\ &+\alpha_\mathrm{p}\left(\bar{P}_{i,\mathrm{opt}}^t - \bar{P}_i^t\right)^2 + \alpha_\mathrm{p}\left(\underline{P}_{i,\mathrm{opt}}^t - \underline{P}_i^t\right)^2 \end{aligned}$$

$$\begin{aligned} L_2^t = &\left(\bar{E}_{i,\mathrm{opt}}^t\right)^2 + \left(\underline{E}_{i,\mathrm{opt}}^t\right)^2 + \\ &+\beta_\mathrm{p}\left(\bar{P}_{i,\mathrm{opt}}^t\right)^2 + \beta_\mathrm{p}\left(\underline{P}_{i,\mathrm{opt}}^t\right)^2 \end{aligned}$$

The first term minimizes the distance between the optimized boundaries and the original AFR-1′ boundaries, while the second term minimizes the fluctuation of the optimized boundaries. Parameters α_p, β, and β_p are all constant coefficients.

The constraints of the optimization problem are as follows:

$$\bar{E}_{i,\mathrm{opt}}^t \geq \underline{E}_{i,\mathrm{opt}}^t, \forall t \in \{1,2,...,T_\mathrm{d}\} \tag{24}$$

$$\bar{P}_{i,\mathrm{opt}}^t \geq \underline{P}_{i,\mathrm{opt}}^t, \forall t \in \{1,2,...,T_\mathrm{d}\} \tag{25}$$

$$\bar{E}_{i,\mathrm{opt}}^t \leq \bar{E}_i^t, \forall t \in \{1,2,...,T_\mathrm{d}\} \tag{26}$$

$$\underline{E}_{i,\mathrm{opt}}^t \geq \underline{E}_i^t, \forall t \in \{1,2,...,T_\mathrm{d}\} \tag{27}$$

$$\bar{P}_{i,\mathrm{opt}}^t \leq \bar{P}_i^t, \forall t \in \{1,2,...,T_\mathrm{d}\} \tag{28}$$

$$\underline{P}_{i,\mathrm{opt}}^t \geq \underline{P}_i^t, \forall t \in \{1,2,...,T_\mathrm{d}\} \tag{29}$$

$$\begin{aligned} &\max_{\boldsymbol{C}\boldsymbol{E}_i \leq \boldsymbol{d}_i} \mathbf{A}_k^\top \boldsymbol{E}_i \leq \boldsymbol{b}_{i,k}, \\ &\forall k \in \{1,2,...,T_\mathrm{d}(T_\mathrm{d}+1)\} \end{aligned} \tag{30}$$

Here, constraints (24)–(25) ensure that the feasible region after optimization is non-empty; constraints (26)–(29) ensure that the optimized boundaries do not exceed the original boundaries of the AFR-1′ model; and constraint (30) ensures that the polytope $\{\boldsymbol{E}_i|\mathbf{C}\boldsymbol{E}_i \leq \boldsymbol{d}_i\}$ is contained within $\{\boldsymbol{E}_i|\mathbf{A}\boldsymbol{E}_i \leq \boldsymbol{b}_i\}$, where $\mathbf{A}_k^\top$ is the k-th row of matrix $\mathbf{A}$, and $\boldsymbol{b}_{i,k}$ is the k-th element of $\boldsymbol{b}_i$. When both $\mathbf{C}$ and $\mathbf{A}$ are constant matrices, $\max_{\boldsymbol{C}\boldsymbol{E}_i \leq \boldsymbol{d}_i} \mathbf{A}_k^\top \boldsymbol{E}_i$ is uniquely determined by $\boldsymbol{d}_i$. To solve this value, we first write its dual problem:

$$\min \boldsymbol{\lambda}_k^\top \boldsymbol{d}_i \tag{31}$$

$$\text{s.t. } \mathbf{C}^\top \boldsymbol{\lambda}_k - \mathbf{A}_k = 0 \tag{32}$$

$$\boldsymbol{\lambda}_k \geq 0 \tag{33}$$

According to duality theory, the objective function of problem (31)–(33) is always greater than or equal to $\mathbf{A}_k^\top \boldsymbol{E}_i$ in (30). When problem (31)–(33) attains minimum, $\mathbf{A}_k^\top \boldsymbol{E}_i$ in (30) attains its maximum. Therefore, the existence of $\boldsymbol{\lambda}_k^\top \boldsymbol{d}_i \leq \boldsymbol{b}_{i,k}$ ensures:

$$\max_{\boldsymbol{C}\boldsymbol{E}_i \leq \boldsymbol{d}_i} \mathbf{A}_k^\top \boldsymbol{E}_i \leq \boldsymbol{\lambda}_k^\top \boldsymbol{d}_i \leq \boldsymbol{b}_{i,k} \tag{34}$$

Thus, (30) is equivalent to:

$$\boldsymbol{\lambda}_k^\top \boldsymbol{d}_i \leq \boldsymbol{b}_{i,k}, \forall k \in \{1,2,...,T_\mathrm{d}(T_\mathrm{d}+1)\} \tag{35}$$

$$\begin{aligned} &\mathbf{C}^\top \boldsymbol{\lambda}_k - \mathbf{A}_k = 0, \\ &\forall k \in \{1,2,...,T_\mathrm{d}(T_\mathrm{d}+1)\} \end{aligned} \tag{36}$$

$$\boldsymbol{\lambda}_k \geq 0, \forall k \in \{1,2,...,T_\mathrm{d}(T_\mathrm{d}+1)\} \tag{37}$$

Let:

$$\boldsymbol{M} = \begin{bmatrix} \boldsymbol{\lambda}_1^\top \\ \boldsymbol{\lambda}_2^\top \\ \cdots \\ \boldsymbol{\lambda}_{T_\mathrm{d}(T_\mathrm{d}+1)}^\top \end{bmatrix} \in \mathbb{R}^{T_\mathrm{d}(T_\mathrm{d}+1)\times 4(T_\mathrm{d}+1)} \tag{38}$$

Then, (35)–(37) can be rewritten as:

$$\boldsymbol{M}\boldsymbol{d}_i \leq \boldsymbol{b}_i \tag{39}$$

$$\boldsymbol{M}\mathbf{C} = \mathbf{A} \tag{40}$$

$$\boldsymbol{M} \geq 0 \tag{41}$$

2.2 Solution method through alternating optimization

In the evaluation mode for obtaining the adjustable capability of a single PSCS derived in last subsection, constraint (39) contains bilinear terms of $\boldsymbol{M}$ and $\boldsymbol{d}_i$. If a day is divided into 96 time intervals ($T_\mathrm{d} = 96$), then the dimension of matrix $\boldsymbol{M}$ reaches 9312 × 388, and the dimension of $\boldsymbol{d}_i$ is 388 × 1. Such a problem cannot be solved efficiently with existing optimization software. Therefore, this paper employs an alternating optimization approach. The algorithm steps are summarized as follows (see Table 2):

Regarding the selection of initial values for boundary parameters, since the outer approximation boundaries of the AFR-1′ model are not far from the exact feasible region boundaries, this paper generates initial boundaries $\boldsymbol{d}_i^0$ by shrinking the parameters of the AFR-1′ model of a single station. The formula is given as follows, where μ is the shrinkage coefficient, typically taken between 0.8 and 0.9:

$$\boldsymbol{d}_i^0 = \begin{bmatrix} \bar{\boldsymbol{E}}_{i,0} \\ -\underline{\boldsymbol{E}}_{i,0} \\ \delta\bar{\boldsymbol{P}}_{i,0} \\ -\delta\underline{\boldsymbol{P}}_{i,0} \end{bmatrix} \tag{42}$$

Table 2
Steps of the alternating optimization.

	Alternating optimization algorithm
step1	Set the maximum number of iterations, convergence tolerance ε, and coefficients of the objective function terms. Compute $\boldsymbol{d}_i^0$, the initial value of vector $\boldsymbol{d}_i$, and let $\boldsymbol{d}_i^{\text{curr}} = \boldsymbol{d}_i^0$.
step2	Substitute $\boldsymbol{d}_i^{\text{curr}}$ into (33), and for all $k \in \{1, 2, ..., T_{\text{d}}(T_{\text{d}}+1)\}$, find $\boldsymbol{\lambda}_k$ that satisfies (35)–(37). Then construct matrix $\boldsymbol{M}^{\text{new}}$ according to (38).
step3	Substitute $\boldsymbol{M}^{\text{new}}$ into (39), and solve problems (23)–(29) and (39) to obtain $\boldsymbol{d}_i^{\text{new}}$.
step4	Check whether the relative error condition $\| \boldsymbol{d}_i^{\text{new}} - \boldsymbol{d}_i^{\text{curr}} \| / \| \boldsymbol{d}_i^{\text{curr}} \| < \varepsilon$ is satisfied. If yes, go to Step 5; otherwise, set $\boldsymbol{d}_i^{\text{curr}} = \boldsymbol{d}_i^{\text{new}}$ and return to Step 2.
step5	Output the iterative results $\boldsymbol{d}_i^{\text{new}}$.

$$\bar{E}_{i,0}^{t} = \frac{\bar{E}_i^t + \underline{E}_i^t}{2} + \mu \frac{\bar{E}_i^t - \underline{E}_i^t}{2} \tag{43}$$

$$\underline{E}_{i,0}^{t} = \frac{\bar{E}_i^t + \underline{E}_i^t}{2} + \mu \frac{\underline{E}_i^t - \bar{E}_i^t}{2} \tag{44}$$

$$\bar{P}_{i,0}^{t} = \frac{\bar{P}_i^t + \underline{P}_i^t}{2} + \mu \frac{\bar{P}_i^t - \underline{P}_i^t}{2} \tag{45}$$

$$\underline{P}_{i,0}^{t} = \frac{\bar{P}_i^t + \underline{P}_i^t}{2} + \mu \frac{\underline{P}_i^t - \bar{P}_i^t}{2} \tag{46}$$

For selecting the weight coefficients in the objective function (23), this paper employs the Bayesian optimization algorithm, commonly used for hyperparameter optimization, to find the values of α_{p}, β, and β_{p} that maximize the feasible region area $\sum_{t=1}^{T_{\text{d}}} \left[\left(\bar{E}_{i,\text{opt}}^t - \underline{E}_{i,\text{opt}}^t \right) + \delta \left(\bar{P}_{i,\text{opt}}^t - \underline{P}_{i,\text{opt}}^t \right) \right]$.

3 Multi-station adjustable capability model considering local security constraints

As shown in Fig. 3, when a VPP (or an aggregator) regulates its aggregated PSCSs, it must ensure local grid security at each station. Specifically, the power at each station must not exceed the capacity limit of its local distribution transformer and line. In addition, stations under the control of a VPP may be geographically proximate and connected to the same substation, resulting in power coupling. At the VPP level, there may also be a maximum total power constraint, such as the capacity limit set by the electricity market trading rules.

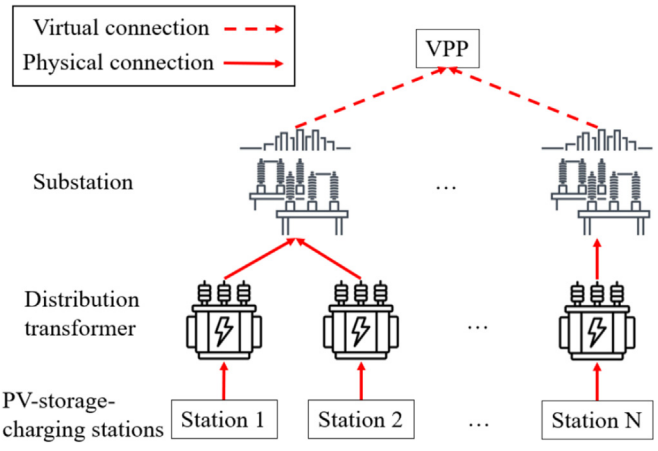

Fig. 3. Illustration of aggregating multiple stations by a VPP.

This paper formulates a two-stage optimization problem to solve for the aggregated power boundaries of a VPP. In stage 1, under the conditions of each station's adjustable boundaries and local security constraints, the upper boundary of the total power across multiple stations is obtained by maximizing (47), and the lower boundary is obtained by minimizing (48).

$$\min \sum_{i \in \Phi^{\text{vpp}}} \sum_{t=1}^{T_{\text{d}}} p_{i,\text{agg}}^t \tag{47}$$

$$\max \sum_{i \in \Phi^{\text{vpp}}} \sum_{t=1}^{T_{\text{d}}} p_{i,\text{agg}}^t \tag{48}$$

$$\underline{P}_i^t \le p_{i,\text{agg}}^t \le \bar{P}_i^t, \forall t \in \{1, 2, ..., T_{\text{d}}\} \tag{49}$$

$$\left| p_{i,\text{agg}}^t \right| \le S_i^{\text{agg}} \cos \varphi_i^{\text{agg}}, \forall t \in \{1, 2, ..., T_{\text{d}}\} \tag{50}$$

$$\left| \sum_{i \in \Phi_v^{\text{sub}}} p_{i,\text{agg}}^t \right| \le S_v^{\text{sub}}, \forall t \in \{1, 2, ..., T_{\text{d}}\} \tag{51}$$

$$\left| \sum_{i \in \Phi^{\text{vpp}}} p_{i,\text{agg}}^t \right| \le S^{\text{vpp}}, \forall t \in \{1, 2, ..., T_{\text{d}}\} \tag{52}$$

The decision variable $p_{i,\text{agg}}^t$ denotes the aggregated total power of i-th PSCS; S_i^{agg} is the capacity of its distribution transformer; $\cos \varphi_i^{\text{agg}}$ is its power factor; Φ_v^{sub} denotes the set of PSCSs connected to substation v; Φ^{vpp} denotes the set of PSCSs managed by the VPP; S_v^{sub} is the residual capacity of substation v after excluding other loads; and S^{vpp} is the possible total capacity limit of the VPP. This problem is a linear optimization model, which can be solved efficiently.

In stage 2, using the optimization results from Stage 1 as benchmarks, the second-stage optimization reduces power fluctuations at each station. The objective is to minimize the sum of squares of power across all time periods:

$$\min \sum_{i\in\Phi^{\mathrm{vpp}}} \sum_{t=1}^{T_{\mathrm{d}}} \left(p_{i,\mathrm{agg}}^{t}\right)^{2} \tag{53}$$

In addition to constraints (49)–(52), the second-stage problem also includes non-inferiority constraints relative to the first-stage results. Specifically, for the upper power boundary, constraint (54) is imposed, and for the lower power boundary, constraint (55) is imposed. Here, $R_1^{\max}$ and $R_1^{\min}$ denote the objective values obtained in the first stage for the upper and lower boundaries, respectively.

$$\sum_{i\in\Phi^{\mathrm{vpp}}} \sum_{t=1}^{T_{\mathrm{d}}} p_{i,\mathrm{agg}}^{t} \geq R_1^{\max} \tag{54}$$

$$\sum_{i\in\Phi^{\mathrm{vpp}}} \sum_{t=1}^{T_{\mathrm{d}}} p_{i,\mathrm{agg}}^{t} \leq R_1^{\min} \tag{55}$$

4 Case study

4.1 Parameter settings

Assume that each day is divided into 96 time intervals, with a convergence tolerance of 10^{-5}. Based on actual information from existing PSCS projects, the capacities of equipment and transformers at each station are set as shown in Table 3. Regarding the station connections, it is assumed that stations A and B are connected to the same substation, whereas station C is connected to another substation. The remaining capacities of substations and the total capacity of the VPP are listed in Table 4.

4.2 Simulation results and analyses

For each station, both the AFR-1′ model boundaries and the improved AFR-2 model-based boundaries are solved. For convenience, the improved AFR-2 model-based boundaries will be simply referred to as AFR-2 in the following discussion. As shown in Fig. 4, the iterative process converges to the predefined tolerance within 10 iterations at all stations, indicating fast computation. Meanwhile, the dual gap of the dual problem is also calculated to verify the optimality of the iterative results. Taking station A as an example, by substituting the obtained $\boldsymbol{d}_{\mathrm{A}}^{\mathrm{new}}$ into (30) and (31)–(33), the objective function values of the primal (z_{pri}) and dual problems (z_{dua}) are derived. The relative dual gap (RDG) is then calculated according to (56), and the average value across all 9312 RDGs is obtained as 2.6619×10^{-17}. This result indicates that the first inequality in (34) can be taken as equality, i.e., both the primal and dual problems achieve optimality within the allowable tolerance.

$$R_{\mathrm{DG}} = \frac{\left|z_{\mathrm{dua}} - z_{\mathrm{pri}}\right|}{\left|z_{\mathrm{dua}}\right| - \left|z_{\mathrm{pri}}\right|} \tag{56}$$

The boundary curves obtained from the iteration are shown in Fig. 5. Table 5 summarizes the feasible region sizes before and after adjustment. The contraction ratio is defined as the compressed area divided by the original area. It can be seen that the feasible region sizes after correction are approximately 80 % of the original values.

To verify that the proposed method can indeed improve the decomposability of total power, a practical application scenario is considered: a PSCS optimize its cost-minimizing guidance power (p_*^t) curve based on the predicted power-energy boundaries and electricity price curves, and then allocate this total power to individual resources in the following day. p_*^t can be obtained by solving problem (57)–(59):

$$\min \sum_{t=1}^{T_{\mathrm{d}}} \rho^t p_*^t \tag{57}$$

$$\text{s.t. } \underline{P}^t \leq p_*^t \leq \bar{P}^t, \forall t \in \{1,2,\ldots,T_{\mathrm{d}}\} \tag{58}$$

$$\underline{E}^t \leq \delta \sum_{\tau=1}^{t} p_*^{\tau} \leq \bar{E}^t, \forall t \in \{1,2,\ldots,T_{\mathrm{d}}\} \tag{59}$$

where ρ^t is the electricity price curve, and the constraints are the power and energy boundaries of the station.

Next, the decomposability of p_*^t is examined by solving optimization problem (60)–(64). Here, $p_{i,j}^t$ denotes the power of resource j in station i at time t, while w_+^t and w_-^t are non-negative slack variables. Constraint (61) ensures that the sum power of all resources within a station, adjusted by slack variables, equals to the guidance power. The objective function minimizes the slack vari-

Table 3
Station settings.

	Station A	Station B	Station C
PV capacity (kW)	100	312	150
Number of EV charging piles	50	8	30
Maximum power of each EV charging pile (kW)	7	60	20
Rated capacity of ESS (MWh)	0.57	15	12.5
Maximum power of ESS (MW)	0.1	3	2.5
Maximum discharge depth of ESS	10 %	10 %	10 %
Capacity of distribution transformer (MW)	1.18	3.1	2.8
Power factor of distribution transformer	0.85	0.85	0.85

Table 4
Substations and VPP capacity settings.

	Capacity (MW)
Remaining capacity of the substation jointly connected by stations A and B	3.1
Remaining capacity of the substation connected by station C	2.3
VPP	5.3

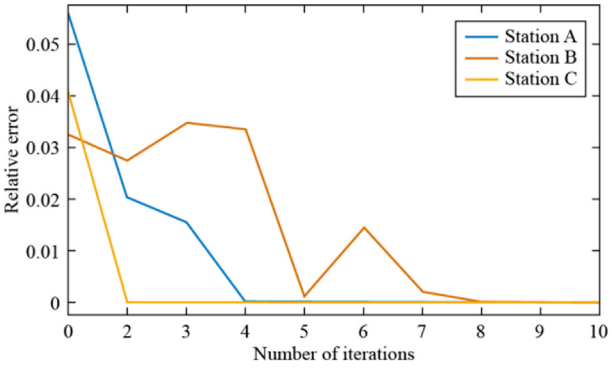

Fig. 4. Iterative convergence process.

ables. Constraints (63)–(64) enforce power and energy boundaries for individual resources, ensuring that the guidance power is allocable to every resource. Finally, the relative error (RE) indicator is calculated according to (65). A larger RE indicates poorer decomposability of p_*^t.

$$\min \sum_{t=1}^{T_d} \left(w_+^t + w_-^t\right) \tag{60}$$

$$\text{s.t.} \sum_{j\in\Phi_i^{sta}} p_{i,j}^t + w_+^t - w_-^t = p_*^t, \quad \forall t \in \{1,2,...,T_d\} \tag{61}$$

$$w_+^t, w_-^t \geq 0, \forall t \in \{1,2,...,T_d\} \tag{62}$$

$$\underline{p}_{i,j}^t \leq p_{i,j}^t \leq \bar{p}_{i,j}^t, \forall j \in \Phi_i^{sta}, \quad \forall t \in \{1,2,...,T_d\} \tag{63}$$

$$\underline{e}_{i,j}^t \leq \delta \sum_{\tau=1}^{t} p_{i,j}^\tau \leq \bar{e}_{i,j}^t, \forall j \in \Phi_i^{sta}, \quad \forall t \in \{1,2,...,T_d\} \tag{64}$$

$$R_E = \frac{\sum_{t=1}^{T_d}\left(w_+^t + w_-^t\right)}{\sum_{t=1}^{T_d}\left|p_*^t\right|} \tag{65}$$

Taking station A as an example, the decomposability of p_*^t obtained from the AFR-1′ boundaries and AFR-2 model-based boundaries is compared. In addition, a series of "intermediate" models are considered for comparison. Their names and meanings are shown in Table 6. For electricity price data, this paper selects ten day-ahead price curves from the Liaoning electricity spot market during August 1st to 10th, 2025 [22]. The RE values are calculated for each curve and then averaged, with results shown in Fig. 6.

It can be observed that the AFR-1′ model exhibits the worst decomposability of p_*^t. As the number of time intervals based on AFR-1′ boundaries decreases, the average RE gradually declines. The AFR-2 model achieves the smallest average RE, with negative values attributed to numerical errors and solver tolerances, which can be considered negligible. Furthermore, when the number of time intervals based on AFR-1′ boundaries is the same, the E-x models exhibit significantly smaller average RE than the B-x and P-x models. For example, E-60, where only the energy boundaries of the first 60 time periods are based on AFR-1′, outperforms B-20 and P-20, where both boundaries and only the power boundaries of the first 20 time periods follow AFR-1′, respectively. This indicates that improving the accuracy of power boundaries is more critical than improving the accuracy of energy boundaries in reducing decomposition errors.

After obtaining the improved power and energy boundaries of each station, the multi-station adjustable capability model considering security constraints is solved. The results of Stage 1 and Stage 2 are shown in Fig. 7. Comparison reveals that the fluctuation of power boundaries is significantly reduced after Stage 2 optimization. In addition, for both Stage 1 and Stage 2, the number of time intervals where the upper power boundary reaches the capacity limit is greater than that of the lower boundary. This is due to the charging demand of EV resources, where the overall charging power exceeds the discharging power.

5 Conclusion

This paper focuses on PSCSs and introduces PEB models for individual resources, including PVs, ESS, and EV charging facilities. An aggregated approximation model based on power and energy boundaries at a single station is analyzed. By embedding low-dimensional models into high-dimensional models, the decomposability of evaluation results is improved. Furthermore, a multi-station aggregation method considering local transformer capacity constraints is proposed.

Through case studies, the effectiveness of the proposed contraction-correction model in enhancing decomposability is verified. Finally, the aggregated power and energy boundaries of multiple stations under security constraints are analyzed, and it is shown that the two-stage model significantly reduces the fluctuation of power boundaries across stations.

Nevertheless, this study has several limitations that should be acknowledged. First, the randomness of EV behavior and PV generation is not considered. Second, the alternating optimization algorithm adopted in this

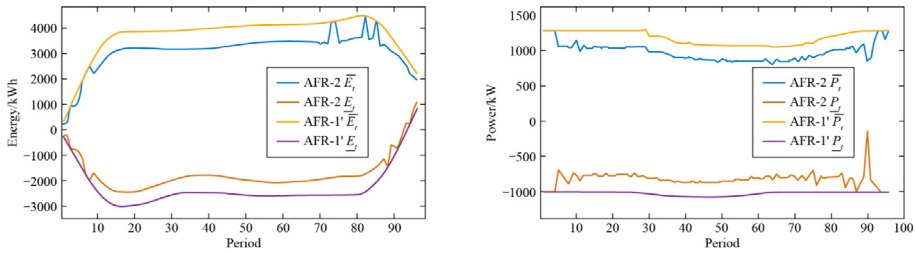

(a) Energy and power boundary results of station A

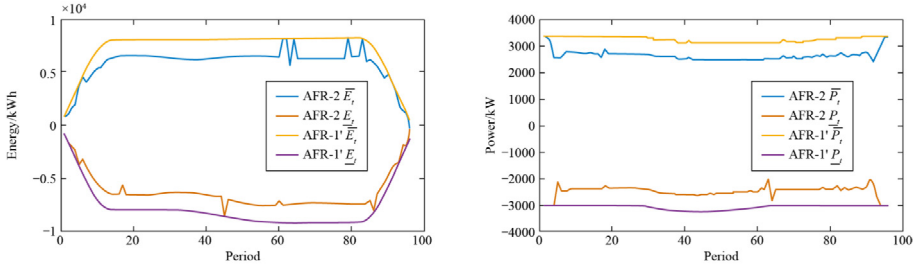

(b) Energy and power boundary results of station B

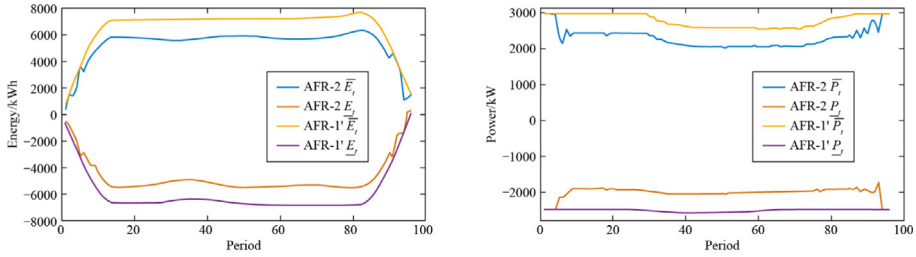

(c) Energy and power boundary results of station C

Fig. 5. Energy and power boundary results of each station.

Table 5
Feasible region area parameters of each station.

	Station A	Station B	Station C
Energy feasible region area of AFR-1′ /MWh	572.39	1434.8	1198.5
Energy feasible region area of AFR-2/MWh	462.08	1159.2	959.78
Contraction ratio of energy feasible region area	80.73 %	80.79 %	80.08 %
Power feasible region area of AFR-1′ /MW	211.31	605.61	512.29
Power feasible region area of AFR-2 /MW	172.46	491.22	417.98
Contraction ratio of power feasible region area	81.62 %	81.11 %	81.59 %

study can guarantee optimality for each iteration but cannot ensure convergence to a global optimum. Third, the security constraints in the multi-station aggregation model are relatively simplified and do not include network-level power-flow constraints. These limitations indicate potential directions for future work, such as constructing AFRs under different confidence levels using historical data, employing relaxation-based techniques to directly

Table 6
Names and meanings of intermediate models.

Names	Meanings
B-x	The power and energy boundaries are both formed by combinations: the first x time periods are consistent with the AFR-1′, while the time periods from x + 1 onwards are consistent with the AFR-2 model.
P-x	Only the power boundary is formed through combination, whereas the energy boundary is exactly the same as the AFR-2 model.
E-x	Only the energy boundary is formed through combination, whereas the power boundary is exactly the same as the AFR-2 model.

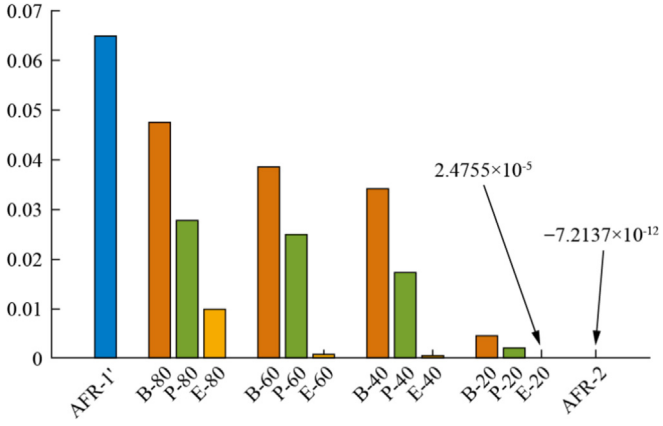

Fig. 6. Average relative error of different models.

approach global optimality, and incorporating linearized power-flow models to better consider network constraints.

CRediT authorship contribution statement

Chao Li: Formal analysis, Data curation, Conceptualization. **Jiawei He:** Writing – original draft, Methodology. **Tingzhe Pan:** Resources. **Zijie Meng:** Data curation. **Xinlei Cai:** Resources. **Xin Jin:** Supervision. **Zechun Hu:** Writing – review & editing, Methodology.

Declaration of competing interest

The authors declare the following financial interests/personal relationships which may be considered as potential competing interests: Chao LI, Zijie MENG and Xinlei CAI are currently employed by Power Dispatching Control Center of Guangdong Power Grid Co., LTD; Tingzhe PAN and Xin JIN are currently employed by CSG Electric Power Research Institute.

Acknowledgement

This work was supported by Science and Technology Project of China Southern Power Grid Company (036000KK52222007(GDKJXM20222121)).

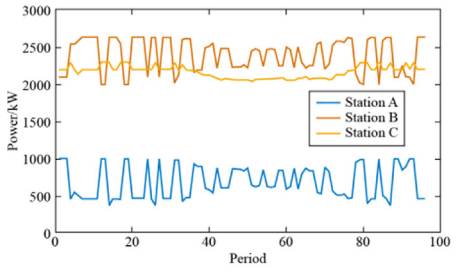

(a) Upper bound of power (stage1)

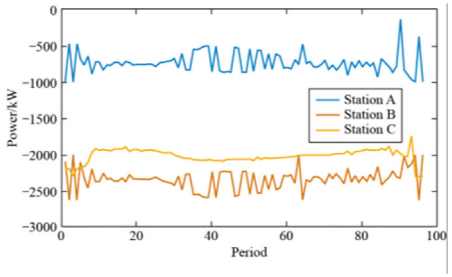

(b) Lower bound of power (stage1)

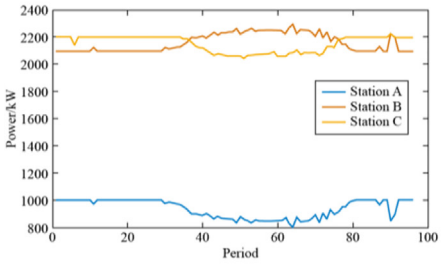

(c) Upper bound of power (stage2)

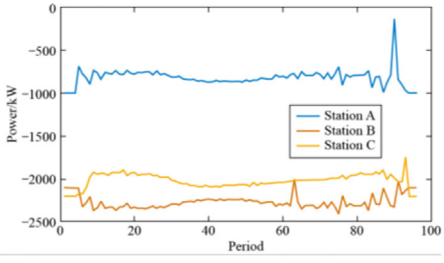

(d) Lower bound of power (stage2)

Fig. 7. Power boundaries of PSCSs considering security constraints.

References

[1] Q. Yan, B. Zhang, M. Kezunovic, Optimized operational cost reduction for an EV charging station integrated with battery energy storage and PV generation, IEEE Trans. Smart Grid 10 (2) (2019) 2096–2106.

[2] M. Alizadeh, A.M. Amani, L. Meegahapola, M. Jalili, O. Hill, Optimal integration of EV charging stations into distribution network planning and operation, IEEE Trans. Ind. Inf. 21 (9) (2025) 7120–7130.

[3] M. Azimi Nasab, M. Alizadeh, R. Nasimov, M. Zand, M. Azimi Nasab, S. Padmanaban, Planning with the electricity market one day ahead for a smart home connected to the RES by the MILP method, Renew. Energy Focus 50 (2024) 100606.

[4] M. Alizadeh, L. Meegahapola, A.M. Amani, M. Jalili, A. Seilsepour, Optimal planning framework for battery energy storage systems and electric vehicle charging stations in distribution networks, in: Proceedings of the IEEE International Conference on Industrial Technology (ICIT), Bristol, United Kingdom, 2024, pp. 1–6.

[5] S.Y. Ge, H.H. Lian, H. Liu, et al., Timing response capability model and control method of electric vehicle, Automat. Electr. Power Syst. 40 (3) (2016) 33–38.

[6] H. Liu, H.H. Lian, S.Y. Ge, et al., Timing response capability model of electric vehicle battery swapping station and strategy formulation of charging plan, Automat Electr. Power Syst. 41 (8) (2017) 91–97.

[7] M. Jenkins, I. Kockar, Electric vehicle aggregation model: a probabilistic approach in representing flexibility, Electr. Pow. Syst. Res. 213 (2022) 108484.

[8] M. Pertl, F. Carducci, M. Tabone, et al., An equivalent time-variant storage model to harness EV flexibility: forecast and aggregation, IEEE Trans. Ind. Inf. 15 (4) (2019) 1899–1910.

[9] F. Al Taha, T.L. Vincent, E. Bitar, An efficient method for quantifying the aggregate flexibility of plug-in electric vehicle populations, IEEE Trans. Smart Grid 16 (4) (2025) 3142–3154.

[10] Z. Yi, Y. Xu, W. Gu, et al., Aggregate operation model for numerous small-capacity distributed energy resources considering uncertainty, IEEE Trans. Smart Grid 12 (5) (2021) 4208–4224.

[11] X.U. Tianyun, C. Tao, Z. Xin, et al., Zonotope based wide-area aggregation and regulation method for distributed resources in virtual power plant, Automat. Electr. Power Syst. 48 (18) (2024) 139–148.

[12] Y. Wen, Z. Hu, J. He, et al., Improved inner approximation for aggregating power flexibility in active distribution networks and its applications, IEEE Trans. Smart Grid 15 (4) (2024) 3653–3665.

[13] R. Lyu, H. Guo, G. Strbac, et al., Data-driven dimension reduction for industrial load modeling using inverse optimization, IEEE Trans. Smart Grid 16 (3) (2025) 2695–2698.

[14] D.A. Contreras, K. Rudion, Computing the feasible operating region of active distribution networks: comparison and validation of random sampling and optimal power flow based methods, IET Generat., Trans. Distribut. 15 (10) (2021) 1600–1612.

[15] Z. Tan, H. Zhong, Q. Xia, et al., Estimating the robust P–Q capability of a technical virtual power plant under uncertainties, IEEE Trans. Power Syst. 35 (6) (2020) 4285–4296.

[16] L. Chen, Z. Tang, S. He, et al., Feasible operation region estimation of virtual power plant considering heterogeneity and uncertainty of distributed energy resources, Appl. Energy 362 (2024) 123000.

[17] X. Chen, N. Li, Leveraging two-stage adaptive robust optimization for power flexibility aggregation, IEEE Trans. Smart Grid 12 (5) (2021) 3954–3965.

[18] S. Wang, W. Wu, Q. Chen, et al., Stochastic flexibility evaluation for virtual power plants by aggregating distributed energy resources, CSEE J. Power Energy Syst 10 (3) (2024) 988–999.

[19] J.L. Mathieu, M. Kamgarpour, J. Lygeros, et al., Arbitraging intraday wholesale energy market prices with aggregations of thermostatic loads, IEEE Trans. Power Syst. 30 (2) (2015) 763–772.

[20] Z. Xu, D.S. Callaway, Z. Hu, et al., Hierarchical coordination of heterogeneous flexible loads, IEEE Trans. Power Syst. 31 (6) (2016) 4206–4216.

[21] Y. Wen, Z. Hu, S. You, et al., Aggregate feasible region of DERs: exact formulation and approximate models, IEEE Trans. Smart Grid 13 (6) (2022) 4405–4423.

[22] Liaoning Provincial Development and Reform Commission (2025) Spot electricity price. https://fgw.ln.gov.cn/fgw/xxgk/xhdj/index.shtml. Accessed 14 Sep 2025.

Chao Li received the Ph.D. degree in electrical engineering and Automation from Huazhong University of Science and Technology, Wuhan, China, in 2020. He is currently an engineer with the Power Dispatching Control Center of Guangdong Power Grid Co., Ltd., Guangzhou, China. His research interests include optimal operation and control of power systems.